Chemical Synthesis

Research Article

Dynamic evolution of HZSM-5 zeolite framework under steam treatment

Lin-Hai He[1,2], Jun-Jie Li[3], Song-Yue Han[1,2], Dong Fan[1], Xiu-Jie Li[3], Shu-Tao Xu[1,*] iD, Ying-Xu Wei[1], Zhong-Min Liu[1,2,3]

[1]National Engineering Research Center of Lower-Carbon Catalysis Technology, Dalian Institute of Chemical Physics, Chinese Academy of Sciences, Dalian 116023, Liaoning, China.
[2]University of Chinese Academy of Sciences, Beijing 100049, China.
[3]State Key Laboratory of Catalysis, Dalian Institute of Chemical Physics, Chinese Academy of Sciences, Dalian 116023, Liaoning, China.

Correspondence to: Prof. Shu-Tao Xu, National Engineering Research Center of Lower-Carbon Catalysis Technology, Dalian Institute of Chemical Physics, Chinese Academy of Sciences, 457 Zhongshan Road, Dalian 116023, Liaoning, China. E-mail: xushutao@dicp.ac.cn

Abstract

Understanding the dynamic evolution of zeolite framework structures and the interactions between various hydroxyl groups or aluminum species under different steam conditions at the atomic scale is extremely crucial. Herein, using a series of characterization methods, the framework structures of HZSM-5 zeolites (Si/Al = 36) following exposure to steam in the temperature range of 100 to 500 °C are investigated. Under mild steam conditions (T ≤ 200 °C), dealumination is nearly absent, and the silanol nests directly condense to create new framework Si-O-Si bonds. Conversely, under severe steam conditions (T ≥ 300 °C), the framework tetrahedral aluminum atoms Al(IV)-1 can be sequentially converted to partially coordinated framework aluminum Al(IV)-2 and extra-framework aluminum (EFAL) through partial and complete hydrolysis, which cause an increase in the framework Si/Al ratio and a decrease in crystallinity. Al(IV)-2 is recognized as a significant intermediate species for framework complete dealumination. The Brønsted acid sites on Al(IV)-2 can be perturbed by the framework Al-OH groups due to hydrogen bonding interactions, leading to a shift in ^{1}H chemical shifts to lower fields, appearing at 6.0-9.0 ppm and 12.0-15.0 ppm. The newly generated EFAL and silanol nests further evolve through condensation as well. Meanwhile, during dealumination, the spatial correlations (or interactions) of various hydroxyl groups on structurally distinct aluminum species [Al(IV)-1, Al(IV)-2, and EFAL] and aluminum species

become extremely intricate. Based on these findings, the dynamic evolution path of HZSM-5 zeolite framework structures under mild and severe steam conditions is proposed.

INTRODUCTION

Zeolites, as vital microporous materials, have garnered substantial attention in both scientific research and industrial engineering. They have been extensively applied for adsorption separation, ion exchange, and heterogeneous catalysis owing to their unique channel structures, tunable acidity properties, and outstanding hydrothermal stability[1-4]. Among the diverse range of zeolites, ZSM-5, with three-dimensional ten-ring pore structures developed by the Mobil company, has shown excellent catalytic performance in many organic catalytic reactions, such as fluid catalytic cracking (FCC)[5], hydrocracking[6], olefin oligomerization[7], alkylation[8], aromatization[9], and methanol-to-hydrocarbon (MTH) conversions[10-12]. The hydrothermal stability of ZSM-5 is a crucial performance factor to consider in its application, mainly because many chemical reactions are often accompanied by the introduction and generation of water; in other words, the real working environments often present different severity of hydrothermal environments[13,14]. During the hydrothermal processes, water molecules inevitably interact with framework aluminum atoms, leading to the structural evolution that significantly affects catalytic performance, including activity, selectivity, and stability. Hence, understanding the dynamic evolution of zeolite framework aluminum atoms under diverse hydrothermal conditions is extremely crucial, which will contribute to a comprehensive insight into the underlying physicochemical process occurring at the water-zeolite interface at the atomic scale.

The degree of changes in zeolite framework structures induced by water molecules depends on the strength of the host-guest interaction between them[15-17]. The interactions range from weak to strong, corresponding to adsorption[18-20], reversible hydrolysis[21-23], and irreversible hydrolysis of framework T-O-T bonds[24-26]. At present, multiple advanced characterization techniques, such as solid-state nuclear magnetic resonance (ss-NMR)[27-29], synchrotron radiation powder X-ray diffraction (SR-PXRD)[30], diffuse reflectance infrared Fourier transform spectroscopy (DRIFTS)[31], X-ray absorption spectroscopy (XAS)[32], and density functional theory (DFT) calculations[25,33,34], are synergistically combined to capture the key species in zeolite dealumination under hydrothermal conditions and analyze their detailed structures. It is widely accepted that the evolution path of framework dealumination is that the Si-O-Al bonds of tetrahedrally coordinated framework aluminum partially hydrolyze with less than four water molecules first to form framework-associated aluminum and then generate EFAL until all four Si-O-Al bonds are hydrolyzed[25,27,33-36]. Framework-associated aluminum is regarded as a critical intermediate species for complete dealumination, and it may revert to the original framework aluminum via dehydration[37]. The generated EFAL species, such as $Al(OH)_3$, $AlOOH$, Al_2O_3, $Al(OH)^{2+}$, $Al(OH)_2^+$, and AlO^+, consist of oxides and multiple hydroxyls, serving as Lewis acid sites that are crucial for zeolite catalytic properties[37-41]. Although the detailed structures of some EFAL species have been proposed on the basis of theoretical calculations, whether they can correspond to the experimental data one by one remains controversial, which strongly hampers the understanding of structure-activity relationships. Notably, EFAL species exhibit complex host-guest interactions with zeolite frameworks. For instance, they can be absorbed near the Brønsted acid sites (BASs) by electrostatic interactions, effectively acting as cations to balance the negative charge of the framework, thereby stabilizing the framework[41]. Yu *et al.* investigated dealuminated HY, HZSM-5, and HMOR zeolites using ^{27}Al double-quantum (DQ) and ^{27}Al multiple-quantum magic-angle spinning (MQMAS) NMR and observed that the three aluminum species, six-, five-coordinate EFAL and four-coordinate framework aluminum species, are in close proximity to each other[27,28]. The resulting Brønsted/Lewis acid synergy effect

can remarkably enhance the acid strength of BASs and further affect the catalytic activity. Recently, using ultra-high field ^{27}Al-^{1}H 2D correlation nuclear magnetic resonance (NMR) experiments, Chen *et al.* discovered the presence of a second protonic acid site in zeolite HZSM-5, specifically the bridge hydroxyl group on the partially bonded framework $(SiO)_{4-n}$-$Al(OH)_n$ species, and further studied its structure in details[42-44]. Similar to traditional BASs, it also exhibits certain catalytic activities, such as significantly increasing catalyst reactivity in benzene hydride-transfer and n-hexane cracking reactions, which has opened new avenues for understanding catalytic mechanisms. It is worth mentioning that accurately identifying the spatial proximity (or interactions) of various hydroxyl groups and aluminum species during hydrothermal dealumination remains a significant challenge and deserves further investigation due to the complexity of these species.

The ss-NMR technique is considered as a powerful tool for investigating the local structure information of zeolites due to its high resolution and non-destructive testing capabilities[45-47]. ^{1}H MAS NMR can distinguish different hydroxyl groups, including Si-OH-Al, Al-OH, and Si-OH groups, in zeolites and directly provide their concentrations[48]. ^{29}Si MAS NMR can be employed to offer the local structure environments around Si atoms and determine the zeolite framework Si/Al ratio[49]. ^{27}Al single-pulse and ^{27}Al MQ MAS NMR can assist in determining the coordination states and concentrations of various aluminum species[50]. Various probe molecules, such as 2-^{13}C-acetone, pyridine-d5, trimethylphosphine (TMP), and TMP oxide (TMPO), are also widely utilized to investigate the acidity, including strength, concentration, and distribution[45,51]. Moreover, many homonuclear and heteronuclear two-dimensional (2D) correlation spectra, such as ^{27}Al-DQ MAS NMR[27,28], ^{1}H-DQ MAS NMR[40], and ^{27}Al-^{1}H heteronuclear multiple quantum correlations (HMQC)[42], have also been used to elucidate the spatial proximity of various hydroxyls and aluminum species in zeolites.

In this contribution, a series of HZSM-5 samples are obtained by accurately controlling the steam temperature for post-treatment with H_2O in a closed reactor. Detailed structures such as the concentrations of different hydroxyls, the coordination states of aluminum species, framework Si/Al ratios, and spatial proximity of both various hydroxyls and aluminum species are investigated qualitatively and quantitatively using a variety of characterization methods. On the basis of experimental data, the dynamic evolution path of framework structures of HZSM-5 zeolites during steam treatment is proposed, which would contribute to a comprehensive insight into the host-guest interactions between zeolite frameworks and water molecules at the atomic scale and the intrinsic hydrothermal stability of zeolites.

EXPERIMENTAL

ZSM-5 zeolite preparation and steam treatment

The ZSM-5 (Si/Al = 36) zeolite was synthesized following the procedure described in the literature[52]. A detailed synthesis description is provided in the Supplementary Material. To obtain HZSM-5 zeolites, calcination at 550 °C for six hours was performed to remove the organic template. The detailed steam treatment of HZSM-5 zeolites followed the approach previously developed by our group[35]. The schematic diagram of high-temperature and high-pressure steam treatment is shown in Supplementary Figure 1. Prior to steam treatment, the HZSM-5 zeolite was dehydrated under vacuum (< 10^{-3} Pa) at 420 °C for over 12 h in a dry quartz tube, and then, it was transferred into a glovebox under a dry argon (Ar) atmosphere for subsequent operations. 10ul deionized water and 50 mg dry HZSM-5 zeolites were added into a quartz tube, separated by a layer of quartz wool. Finally, the quartz tube was placed into a stainless autoclave to seal, and the autoclave was further placed in a muffle furnace and heated at different temperatures (T = 100, 200, 300, 400, and 500 °C) for a period of times. The treated samples were named HZSM-5-T-X (T and X represent the heating temperature in degrees Celsius and heating times in hours, respectively). Note that the untreated

HZSM-5 zeolite was named as HZSM-5. Furthermore, the steamed samples were converted into the ammonium form through ammonium ion exchange, denoted as HZSM-5-T-X-NH$_4$, as detailed in the Supplementary Material.

Characterization

The powder X-ray diffraction (XRD) patterns were recorded on a PANalytical X'Pert PRO X-ray diffractometer with Cu Kα radiation (λ = 1.5418 Å, 40 kV, 40 mA) to confirm the MFI-type topology structure of the samples. The chemical compositions of the samples were measured on an X-ray fluorescence (XRF) spectrometer (Philips Magix-601). The crystal morphology and particle size of the samples were characterized by field emission scanning electron microscopy (FE-SEM, Hitachi, TM3000). The N$_2$ adsorption-desorption experiments were performed to obtain more information about the pore structure at 77 K (Micromeritics ASAP 2020). The temperature-programmed desorption of ammonia (NH$_3$-TPD) was carried out with a Micromeritics Autochem II 2920 analyzer. Subsequently, 150 mg samples were outgassed at 550 °C for 1 h under helium flow, then cooled to 100 °C and exposed to NH$_3$ to saturate the adsorption. The desorption process was carried out from 100 to 800 °C. Fourier transform infrared (FTIR) spectra were recorded on a Nicolet IS50 FTIR spectrometer. The samples (about 5 mg) were pressed into a self-supporting wafer and placed into a quartz cell. Before the measurement, the samples were pretreated at 300 °C for 1 h under vacuum, and then, the spectrum was recorded immediately after the pretreatment.

^{1}H, ^{27}Al, and ^{29}Si MAS NMR and ^{1}H-^{29}Si cross-polarization (CP) MAS NMR experiments were performed on a Bruker Avance NEO 500 spectrometer equipped with 11.7 T and 89 mm wide-bore magnet using a 3.2 mm H/F-X-Y triple resonances MAS probe with the corresponding Larmor frequency of 500.13 MHz, 130.32 MHz, and 99.36 MHz for ^{1}H, ^{27}Al, and ^{29}Si, respectively. Prior to all ^{1}H MAS NMR, the samples were dehydrated under vacuum (< 10^{-3} Pa) at 420 °C for over 12 h in a dry quartz tube connected to a vacuum line and then were transferred into 3.2 mm NMR rotors (tightly sealed by a Kel-F cap) under a dry Ar atmosphere in a glovebox. The chemical shifts of ^{1}H NMR were referenced to adamantane at 1.74 ppm. ^{1}H MAS NMR spectra were performed with a π/2 pulse width of 3.8 μs, a recycle delay of 70 s, and a spinning rate of 20 kHz. The chemical shift of ^{27}Al NMR was referenced to 1 mol/L Al(NO$_3$)$_3$ solution at 0 ppm. ^{27}Al MAS NMR spectra were performed with a pulse width of 0.63 μs (π/18), a recycle delay of 0.5 s, and a spinning rate of 20 kHz. The chemical shifts of ^{29}Si NMR were referenced to kaolinite at -91.5 ppm. ^{29}Si MAS NMR spectra were performed with high-power proton decoupling using a π/4 pulse width of 2.5 μs, a recycle delay of 10 s, and a spinning rate of 10 kHz. ^{1}H-^{29}Si CP MAS NMR spectra were performed with a contact time of 3 ms, a recycle time of 2 s, and a spinning rate of 10 kHz. The decoupling field of 69.4 kHz was applied during the acquisition time.

We conducted several experiments on 2D ^{1}H-^{1}H DQ-SQ MAS NMR, ^{1}H-^{27}Al symmetry-based rotational-echo saturation-pulse double-resonance (S-RESPDOR) MAS NMR, and ^{27}Al MQ MAS NMR on a Bruker Avance III 600 spectrometer equipped with 14.1 T and 89 mm wide-bore magnet using a 3.2 mm H-X-Y triple resonance MAS probe with the corresponding Larmor frequencies of 600.13 MHz and 156.38 MHz for ^{1}H and ^{27}Al, respectively. For the 2D ^{1}H-^{1}H DQ-SQ MAS NMR experiments, we employed the POST-C7 pulse sequence, accumulating either 128 or 400 scans for each of the 64 points in t1 dimensions with an increment time of 41.67 μs, a recycle delay of 2 s, and a spinning rate of 12 kHz. In the case of ^{1}H-^{27}Al S-RESPDOR spectra, we implemented a recycle delay of 10 s and a spinning rate of 20 kHz. For the ^{1}H channel, we applied a π/2 pulse width of 3.2 μs and a π pulse width of 6.4 μs using SR4 recoupling. The recoupling time ranged from 0.2 to 1.0 ms, with intervals of 0.2 ms. The saturation pulse on the ^{27}Al channel was with a duration of 75 μs (1.5 Tr). ^{27}Al MQ MAS NMR spectra were obtained using the z-filter 3QMAS pulse sequence. The pulse durations were set to 4.2 μs and 1.4 μs for the first and second pulse, and the pulse width of the selective pulse was set to 15 μs. Additionally, 3000 or 15000 scans were accumulated for each of

the 64 points in t1 dimensions with an increment time of 50 μs, a recycle delay of 0.1 s, and a spinning rate of 20 kHz. The pulse sequences are shown in Supplementary Figure 2A-C.

We conducted 2D ^{27}Al-^{27}Al DQ-SQ MAS NMR experiments on a Bruker Avance III 600 spectrometer equipped with 14.1 T and 89 mm wide-bore magnet using a 4.0 mm H-X double resonance MAS probe. DQ coherences were excited and reconverted using the BR2$^1_2$ pulse sequence with $\tau_{exc} = \tau_{rec} = 571.43$ μs. CT-selective π/2 and π pulse widths of 11 μs and 22 μs, a recycle delay of 0.1 s, and a spinning rate of 14 kHz were used for the ^{27}Al-^{27}Al DQ-SQ MAS NMR experiments. Furthermore, 40,960, 64,000,120,000, and 128,000 scans were accumulated for each of the 32 points in t1 dimensions with an increment time of 35.71 us for the HZSM-5, HZSM-5-300-24, HZSM-5-400-2, and HZSM-5-500-2 samples, respectively. The pulse sequence is shown in Supplementary Figure 2D.

RESULTS AND DISCUSSION

Structural transformation of HZSM-5 zeolite before and after steam treatment

A series of untreated and steam-treated HZSM-5 samples are characterized by XRD and scanning electron microscopy (SEM). The similar XRD patterns [Supplementary Figure 3A] of the HZSM-5-T-X samples indicate that the MFI-type topology is still maintained after high-temperature and high-pressure hydrothermal treatment. However, as the temperature rises to 200 °C, the peak at 24.4 °C split into a double peak [Supplementary Figure 3B], representing clear evidence for transition of the MFI-type structure from orthorhombic to monoclinic symmetry with 12 and 24 distinguishable framework T sites, respectively[53-55]. This phenomenon can be explained by a mutual shift of successive (010) pentasil layers along [001], which is closely related to the distortion or rotation of the T_4 and T_6 rings interconnecting the pentasil layers[56]. Typically, this transformation is influenced by the Si/Al ratio in the lattice or the adsorption of molecules within ZSM-5 and can be measured by ^{29}Si MAS NMR[57,58]. In addition, taking HZSM-5 as a reference, the relative crystallinity does not start to decrease until the hydrothermal temperature rises to 400 °C, with the lowest value being 87% at 500 °C [Table 1], indicating that harsh hydrothermal treatment can cause the degradation of the MFI-type framework. The morphology and size of particles exhibit no significant changes before and after steam treatment, as can be seen from SEM images [Supplementary Figure 4]; yet, this does not necessarily imply the preservation of zeolite framework microstructure at the atomic level.

^{27}Al MAS NMR is a potential tool for tracking the dynamic evolution of aluminum species during hydrothermal dealumination[29,59]. ^{27}Al single-pulse MAS NMR spectra of the pristine and steam-treated HZSM-5 samples are recorded, as shown in Figure 1A. For HZSM-5 samples, a solitary signal at 55 ppm is evident, representing the framework tetrahedral-coordinated Al species, denoted as Al(IV)-1[43]. When the steam temperature is below 200 °C, the main signal at 55 ppm remains nearly constant in intensity. However, upon reaching 300 °C, the intensity of Al(IV)-1 slightly decreases, accompanied by the emergence of a weak broad signal at 45 ppm. Following treatment at 400 or 500 °C, the intensity of Al(IV)-1 significantly diminishes, and two distinct signals gradually emerge at 30 ppm and 0 ppm, increasing in intensity as Al(IV)-1 decreases. The signals at 30 ppm and 0 ppm are assigned to the penta-coordinated Al and the octahedral-coordinated Al, respectively. Both the penta-coordinated and octahedral-coordinated Al species remain apparent, with minimal changes in relative content, after back exchanging to their ammonium form [Supplementary Figure 5], implying that they can be considered as EFAL species rather than framework-associated Al[37]. Nevertheless, note that ^{27}Al is a nucleus with S = 5/2, and its resolution is limited due to the residual second-order quadrupole broadening that is not entirely eliminated by magic-angle spinning. Therefore, in order to qualitatively identify the Al species in different chemical environments better, the combination of ^{27}Al MQ MAS NMR is indispensable[43,60,61]. The MQ MAS NMR method, proposed by Frydman and Harwood, is capable of refocusing second-order quadrupole effects,

Table 1. Relative crystallinity and textural properties of HZSM-5 zeolites before and after steaming

Samples	C_{XRD}^a (%)	S_{BET}^b (m²/g)	S_{Micro}^c (m²/g)	S_{Ext}^d (m²/g)	V_{Total}^e (cm³/g)	V_{Micro}^f (cm³/g)	V_{Meso}^g (cm³/g)
HZSM-5	100	393	221	172	0.207	0.097	0.110
HZSM-5-100-2	103	393	219	174	0.206	0.100	0.106
HZSM-5-200-2	99	403	207	196	0.210	0.092	0.118
HZSM-5-300-2	101	400	174	226	0.207	0.077	0.130
HZSM-5-400-2	91	348	139	209	0.199	0.068	0.131
HZSM-5-500-2	87	328	166	162	0.196	0.084	0.112

[a]Taking the HZSM-5 as a reference, the relative crystallinity was determined by the diffraction peak area ratio of 22.5-25.0 °C in the XRD spectra; [b]BET Method; [c,f]t-plot method; [d]$S_{Ext} = S_{BET} - S_{Micro}$; [e]$P/P_0 = 0.975$; [g]$V_{Meso} = V_{Total} - V_{Micro}$.
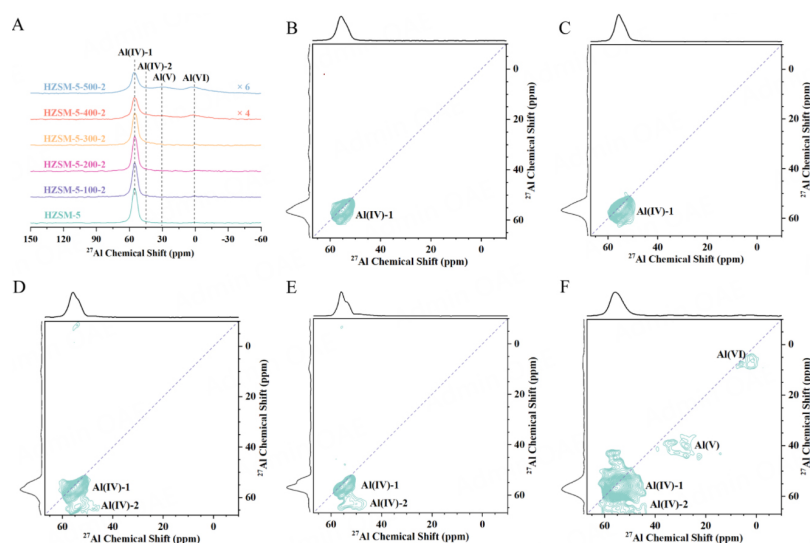

Figure 1. (A) ^{27}Al single-pulse MAS NMR spectra of HZSM-5 before and after steam treatment at 100 ~ 500 °C for 2 h. Note that the intensities have been normalized by mass. ^{27}Al MQ MAS NMR spectrum of HZSM-5 (B); HZSM-5-200-2 (C); HZSM-5-300-2 (D); HZSM-5-300-2-NH$_4$ (E) and HZSM-5-500-2 (F). All samples are fully hydrated.

thereby obtaining the isotropic high-resolution spectrum of half-integer quadrupole nuclei, such as ^{17}O, ^{23}Na, and ^{27}Al[62]. NMR parameters of different Al species extracted from ^{27}Al MQ MAS NMR spectra are listed in Supplementary Table 1. In the ^{27}Al MQ MAS NMR spectra of HZSM-5 [Figure 1B] and HZSM-5-200-2 [Figure 1C], only the Al(IV)-1 signal remains present, illustrating that dealumination does not occur under mild steam conditions. When the temperature increases to 300 °C, as shown in Figure 1D and Supplementary Figure 6, a new broad signal emerges around 45 ppm, exhibiting a larger quadrupole coupling constant ($C_Q = 5.90$ MHz), attributed to the partially bonded framework $(SiO)_{4-n}$-Al(OH)$_n$ species, denoted as Al(IV)-2, demonstrating the irreversible hydrolysis of the first framework Al-O bond is achieved.[42] Prolonging the steam treatment time at 300 °C to 24 h [Supplementary Figure 5], the content of Al(IV)-2 increases and EFAL at 0 and 30 ppm appears, signifying that Al(IV)-2 is a critical intermediate species for the complete dealumination of the framework. Surprisingly, Al(IV)-2 persists distinctly, with minimal changes in relative content, even after exchanging HZSM-5-300 into ammonium form, as shown in Supplementary Figure 5 and Figure 1E. This implies that the transformation from Al(IV)-2 to Al(IV)-1 is not achievable through ammonium exchange treatment. This phenomenon differs from the reversible octahedral–tetrahedral coordination transformation observed in the adsorption of water framework-associated Al[63]. After treatment at 400 or 500 °C, the same phenomenon is observed [Figure 1A and F], with the extent of dealumination escalating as the hydrothermal conditions become more severe. Hence,

both hydrothermal temperature and time are the primary factors affecting the stability of the zeolite framework. It is not difficult to obtain the dynamic evolution path of the framework tetrahedrally coordinated Al atom in severe hydrothermal environments: the four framework Al-O bonds bonded to a framework Al atom partially hydrolyze to form Al(IV)-2 first, and subsequently, the Al atom can be removed from the framework to generate EFAL until all the four framework Al-O bonds are completely hydrolyzed by water molecules.

To gain further insight into the local structural environments surrounding Si atoms, ^{29}Si MAS NMR [Figure 2A] is adopted. Five primary peaks at -103, -106.5, -110, -113, and -116 ppm are observed in all the samples from low to high fields. The signal at -103 ppm can be attributed to Q^3 [Si(OSi)$_3$(OH)] species[29,64], whose intensity can be obviously enhanced in ^{1}H-^{29}Si CP MAS NMR spectra [Supplementary Figure 7] through the transfer of magnetization from dipolar-coupled ^{1}H to ^{29}Si. Correspondingly, the peak at -106.5 ppm is ascribed to Si1Al (Si(OSi)$_3$(OAl)) species[29,64], and its relative percentage is nearly unchanged after steaming at 100 °C and 200 °C for two hours [Figure 2B and Supplementary Table 2]. In other words, there is a slight change in the framework Si/Al ratio, which is about 37, demonstrating that mild steam conditions do not cause irreversible hydrolysis of the framework. In contrast, its relative percentage begins to decline from 10.78% to 2.96% after severe steam treatment at temperatures ranging from 300 °C to 500 °C [Figure 2B and Supplementary Table 2], accompanied by a substantial increase in the framework Si/Al ratio from 37 to 135, suggesting that harsh steam conditions can cause the irreversible hydrolysis of the framework Si-O-Al bonds. The peaks at -110 ppm, -113 ppm, and -116 ppm are all assigned to Q^4 (Si(OSi)$_4$) species[29,64], and their total relative percentage increases from 88.56% to 96.88% as the temperature rises to 500 °C [Figure 2B and Supplementary Table 2], demonstrating dealumination and healing of defects sites occur simultaneously. It is noteworthy that the resolution of ^{29}Si MAS NMR spectra is enhanced after steaming at 400 °C and 500 °C, which can be ascribed to the transition from the orthorhombic to monoclinic symmetries, the reduction of defect Si sites, and the improvement of Si/Al by dealumination procedures[57,65]. The presence of defect Si sites and Al atoms in zeolites can induce a distribution of Si-O bonds and Si-O-Si angles, which broaden the spectral lines and obscure the detection of various crystallographically distinct T sites. These findings are consistent with the results obtained from XRD [Supplementary Figure 1] and ^{27}Al MAS NMR [Figure 1] mentioned above.

In order to identify the dynamic evolution of hydroxyl groups, ^{1}H MAS NMR spectroscopy and FTIR are employed. ^{1}H MAS NMR spectra are recorded [Figure 3A] to quantify the concentrations of various hydroxyl groups by deconvolution. The signals at 3.9, 2.0, and 1.7 ppm are assigned to the unperturbed BAS, geminal or vicinal Si-OH groups, and isolated Si-OH groups, respectively[66,67]. Generally, the signal at 2.5 ppm is attributed to Al-OH groups that exist extra-lattice or EFAL, most likely as small aluminum oxide moieties[67]. Notably, this signal has been verified as framework Al-OH groups on Al(IV)-2 in HZSM-5 zeolites but not EFAL in recent studies[42,43]. Additionally, this signal can also be assigned to water molecules belonging to Al(OH)$_n$(H$_2$O) species from EFALs or external surface sites and hydrogen-bonded silanols[68-71]. Therefore, the precise assignment of this signal remains controversial. In view of this, its attribution is discussed below. Furthermore, the assignment of the broad shoulder peak at 4.6 ppm is relatively complex and remains controversial. So far, it has been assigned to hydrogen-bonded BAS[72,73], residual water[74], and hydrogen-bonded silanols[70] in previous studies. Consequently, a more detailed discussion regarding its assignment is provided below. The broad signal at 12.0-15.0 ppm can be assigned to the BAS on Al(IV)-2[42,43]. Obviously, the concentration of the total hydroxyl groups gradually decreases from 0.498 mmol/g to 0.105 mmol/g as the temperature increases to 500 °C [Figure 3B and Supplementary Table 3], indicating the occurrence of hydroxyl condensation. After mild steam treatment (T ≤ 200 °C), the concentration of BAS at 3.9 ppm remains essentially stable at around 0.1 mmol/g. However, interestingly,
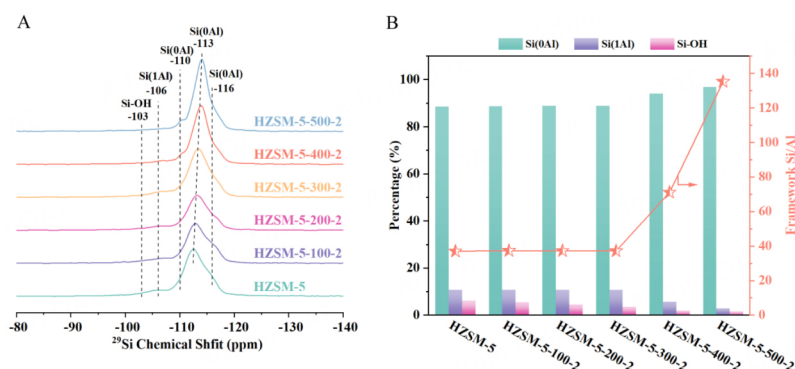
Figure 2. (A) ^{29}Si MAS NMR spectra of HZSM-5 before and after steam treatment; (B) relative percentage of Si species in different chemical environments by deconvolution of ^{29}Si MAS NMR spectra.
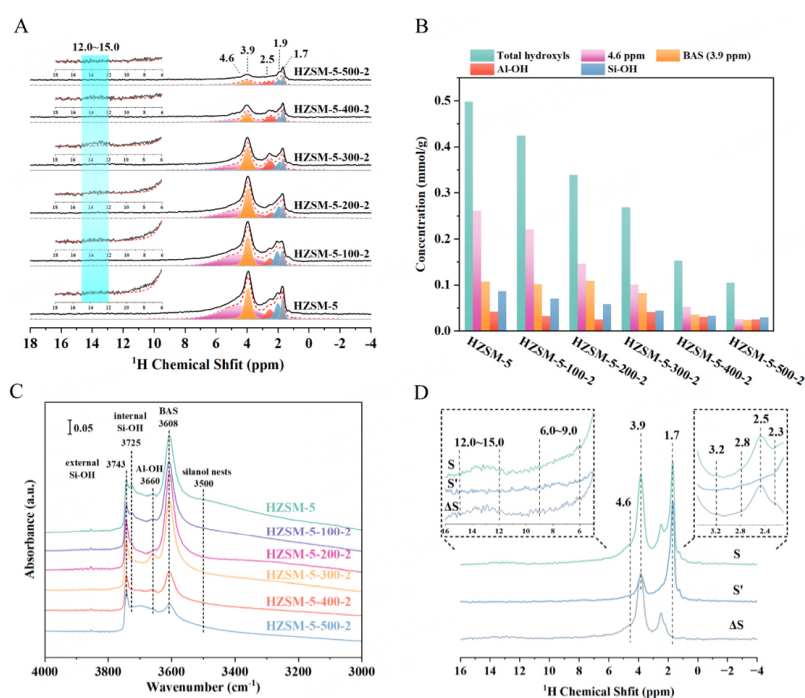

Figure 3. (A) ^{1}H MAS NMR spectra of HZSM-5 before and after steam treatment; (B) concentrations of different hydroxyl groups by quantifying and fitting the quantitative ^{1}H MAS NMR spectra; (C) FTIR spectra of the OH vibration region of HZSM-5 before and after steam treatment; (D) ^{1}H-^{27}Al S-RESPDOR spectra of HZSM-5-300-2 sample with a recoupling time of 0.6 ms. S and S' denote the ^{1}H spectrum without and with ^{27}Al irradiation, respectively; ΔS is the difference spectrum obtained by S-S'.

the concentration of the broad shoulder peak at 4.6 ppm decreases significantly from 0.262 mmol/g to 0.146 mmol/g. Considering the framework Si/Al ratio remains relatively constant, as indicated by ^{29}Si NMR [Figure 2], and no other Al species besides Al(IV)-1 are observed in ^{27}Al NMR [Figure 1A-C], this situation mentioned above can be attributed to the condensation of numerous silicon hydroxyl groups that are inevitably generated during synthesis and calcination. This is further corroborated by the IR results below. Upon reaching 300 °C, the concentrations of Al-OH groups at 2.5 ppm and another broad signal at 12.0-15.0 ppm reach the maximum, but only Al(IV)-2 is generated from ^{27}Al NMR [Figure 1A and D], indicating the signal at 2.5 ppm is related to Al(IV)-2. Meanwhile, the internuclear ^{1}H-^{27}Al distance of this signal is 2.05 ± 0.11 Å by the ^{1}H-^{27}Al S-RESPDOR experiments [Supplementary Figure 8], indicating that the proton is

closely bound to Al atoms. Therefore, it is reasonable to attribute this signal to the framework Al-OH group on Al(IV)-2, consistent with recent studies[42,43,68]. Severe steam treatment (T ≥ 300 °C) can induce framework dealumination, which has been demonstrated by ^{27}Al and ^{29}Si MAS NMR [Figures 1 and 2]. Strangely, only the signal at 2.5 ppm is observed in ^{1}H NMR of dealuminated HZSM-5 zeolites, with no additional new signals emerging. This prompts the consideration that Al-OH groups on EFAL may also contribute to the signal at 2.5 ppm. This possibility cannot be ruled out entirely. That is, the signal at 2.5 ppm cannot be simply attributed to Al-OH groups on EFAL or Al(IV)-2 species and requires thorough analysis alongside ^{27}Al and ^{29}Si NMR. Undeniably, the enhancement of the signal at 2.5 ppm is indicative of the irreversible hydrolysis of the Si-O-Al bonds. In principle, the complete removal of a framework Al atom should result in an Al(OH)$_3$·H$_2$O group and a silicon nest consisting of four silicon hydroxyl groups with hydrogen bonding interactions. Unexpectedly, the concentrations of Al-OH groups and Si-OH groups significantly decrease, which can occur through the condensation reaction from the hydroxyl groups bonded on Al atoms, forming new EFAL species with fewer hydroxyl groups, and from the expected four Si-OH groups (silanol nest) forming new framework Si-O-Si bonds, respectively[75]. The condensation of Al-OH groups causes the diversity of EFAL, such as Al(OH)$_3$, Al(OH)$_2^+$, Al(OH)$^{2+}$, AlO$^+$, Al$_2$O$_3$, dimers, trimers, *etc*. The formation of Si-O-Si bonds may be caused by the direct condensation of adjacent Si-OH groups in the silanol nest and the migration of Si(OH)$_4$ species formed by desilication to the silanol nest for reorganization. The former may be under mild hydrothermal conditions, where desilication is improbable. However, severe hydrothermal conditions may cause the removal of Si atoms from the framework, making the latter possibility plausible.

Infrared (IR) spectra are also utilized to further investigate the dynamic evolution of hydroxyl groups, as shown in [Figure 3C]. In this spectra, five main IR bands are observed in the region of 3,800-3,400 cm^{-1}. The bands at 3,743 cm^{-1}, 3,725 cm^{-1}, 3,608 cm^{-1}, and 3,500 cm^{-1} are ascribed to external Si-OH groups, internal Si-OH groups, BASs, i.e., Si(OH)Al groups, and silanol nests, respectively[76]. The band at 3660 cm^{-1} can be assigned to Al-OH groups on EFAL[77,78] or partially framework-bonded Al species[79,80], but this remains controversial. It can be found that mild steam treatment (T ≤ 200 °C) does not decrease the intensity at 3,743 cm^{-1}, 3,660 cm^{-1}, and 3,608 cm^{-1} but significantly decreases the intensity at 3,725 cm^{-1} and 3,500 cm^{-1}, which is indicative of selective removal of Si-OH groups. This observation is consistent with ^{1}H MAS NMR results and provides further evidence that the silanol nests, hydrogen-bonded silanols, contribute to a portion of the broad shoulder peak at 4.6 ppm in ^{1}H MAS NMR spectra. After steam treatment at 300 °C, the intensity of the band at 3660 cm^{-1} remarkably increases. Given that only Al(IV)-2 is generated from ^{27}Al NMR [Figure 1A and D], the band at 3,660 cm^{-1} can be attributed to Al-OH groups on Al(IV)-2 and is associated with the signal at 2.5 ppm in ^{1}H NMR. The lower intensity of the band at 3608 cm^{-1} for severe steam conditions (T ≥ 300 °C) suggests that less framework tetrahedral Al compared to HZSM-5, in agreement with the lower Al(IV)-1 in ^{27}Al MAS NMR [Figure 1A] and the higher framework Si/Al ratio in ^{29}Si MAS NMR [Figure 2B]. Similarly, the intensity of the band at 3660 cm^{-1} gradually decreases. It is worth mentioning that no additional vibrational bands belonging to Al-OH groups on EFAL species are observed in dealuminated HZSM-5 zeolites, which is a puzzling observation. Therefore, it is reasonable to speculate that the band at 3,660 cm^{-1} represents the superposition of Al-OH groups on Al(IV)-2 and EFAL species.

The acidic properties are examined through NH$_3$-TPD experiments, as shown in Supplementary Figure 9. The two ammonium-desorption peaks at around 470 and 680 K are typically attributed to NH$_3$ desorption from weak and strong acid sites, respectively[76]. Evidently, the temperature and intensity of these two ammonium-desorption peaks remain nearly unchanged after mild steam treatment (T ≤ 200 °C) but gradually decrease as the temperature increases (T ≥ 300 °C). It can be inferred that the weakening of acid strength is a consequence of dealumination, possibly linked to changes in the local chemical environment.

The changes in textural properties induced by steaming are studied by N_2 adsorption experiments [Supplementary Figure 10A]. The isotherms of HZSM-5 steamed at no higher than 300 °C can be considered as a combination of type I and type IV isotherms, while the isotherms of HZSM-5 steamed at 400 and 500 °C can be regarded as type V isotherms. The textural properties of these samples are summarized in Table 1. As expected, the micropore volume remains essentially unchanged after mild steam treatment (T ≤ 200 °C); however, it obviously decreases after severe steam treatment (T ≥ 300 °C), which can be explained by EFAL blocking the channels. Interestingly, despite a more pronounced degree of dealumination at 500 °C compared to 400 °C, the micropore volume and surface slightly increase and the pore diameter is smaller [Table 1 and Supplementary Figure 10B], which may be related to the restructuring of amorphous Si species generated by desiliconation.

Identification of spatial proximity of various hydroxyl species

In order to determine the spatial proximity (or interaction) between different hydroxyls and Al species, the ^{1}H-^{27}Al S-RESPDOR experiment is conducted on HZSM-5-300-2, as shown in Figure 3D. Under ^{27}Al irradiation, the ^{1}H signal of protons that are in close proximity to ^{27}Al atoms will be modulated by ^{1}H-^{27}Al dipolar interaction. Only the protons observed in the difference spectrum (ΔS), acquired by subtracting the ^{1}H MAS NMR spectrum with ^{27}Al irradiation (S') from that without ^{27}Al irradiation (S), have a dipolar interaction with Al atoms. In the difference spectrum [Figure 3D], the ^{1}H signals from BAS at 3.9 ppm, Al-OH at 2.5 ppm, three newly observed signals at 2.3 ppm, 2.8 ppm, and 3.2 ppm, along with three broad signals at 4.6 ppm, 6.0-9.0 ppm, and 12.0-15.0 ppm, are all discernible due to direct ^{1}H-^{27}Al dipole-dipole interactions; that is to say, the protons of these signals are close to the Al species. In contrast, there is no ^{1}H signal from Si-OH at 1.7 ppm in the difference spectrum. Note that the broad shoulder peak at 4.6 ppm with direct ^{1}H-^{27}Al dipole-dipole interaction can be assigned to hydrogen-bonded BAS[73]. Combining the quantitative results of ^{1}H MAS NMR spectra and IR data, this broad signal at 4.6 ppm observed in ^{1}H MAS NMR spectra is at least produced by the superposition of hydrogen-bonded silanols and BAS, in line with previous studies[70,72,73]. Besides, the three signals at 2.3, 2.8, and 3.2 ppm can be tentatively assigned to Al-OH groups, but their detailed structures are still unclear due to the diversity of Al-OH groups in zeolites.

To gain a deeper insight into the dynamic evolution and spatial proximity (or interaction) of different hydroxyl groups within the HZSM-5 zeolite framework during the hydrothermal process under high-temperature and high-pressure conditions, 2D ^{1}H-^{1}H DQ MAS NMR is adopted. This technique has been previously proven effective for obtaining spatial proximity information between various hydroxyl groups with proton-proton distances less than 5Å in a variety of zeolites, such as HZSM-5, HSSZ-13, HMOR, HY, *etc.*[28,35,40]. Peaks that appear along the diagonal represent the autocorrelation peaks (ω, 2ω) resulting from the dipolar interaction of the proton species with the same chemical environment, while paired peaks that appear off-diagonal at (ω$_a$, ω$_a$ + ω$_b$) and (ω$_b$, ω$_a$ + ω$_b$) represent the correlations between proton species with different chemical shifts. Figure 4 shows the 2D ^{1}H-^{1}H DQ-SQ MAS NMR spectra of HZSM-5 before and after steaming. For clarity, all ^{1}H signals appearing from the high to low field are relabeled with letters from A to H, corresponding to the following chemical shifts: 1.7 ppm (A), 2.3 ppm (B), 2.5 ppm (C), 2.8 ppm (D), 3.2 ppm (E), 3.7 ppm (F), 6.0-9.0 ppm (G), and 12.0-15.0 ppm (H). For HZSM-5, two autocorrelation peaks (A-A and F-F) and one off-diagonal peak pair (C-H) are clearly observed in Figure 4A. The one autocorrelation peak (A-A) appearing at (1.7, 3.4) ppm corresponds to the spatial proximity between nonacidic silanol groups. Another autocorrelation peak (E-E) at (3.7, 7.4) ppm suggests that the bridge hydroxyl groups (Si-O(H)-Al) are not isolated but with spatial proximity, which is further supported by the following 2D ^{27}Al-^{27}Al DQ-SQ MAS NMR experiments [Figure 5]. This phenomenon can be explained by the non-homogeneous distribution of framework Al, considering that each unit cell has only 2.6 Al atoms calculated from the Si/Al of 36. The one off-diagonal peak pair (C-H) at (2.5, 14.5-17.0) and (12.0-14.5, 14.5-17.0) ppm is attributed to the correlation between framework Al-OH groups and BAS on Al(IV)-2 species
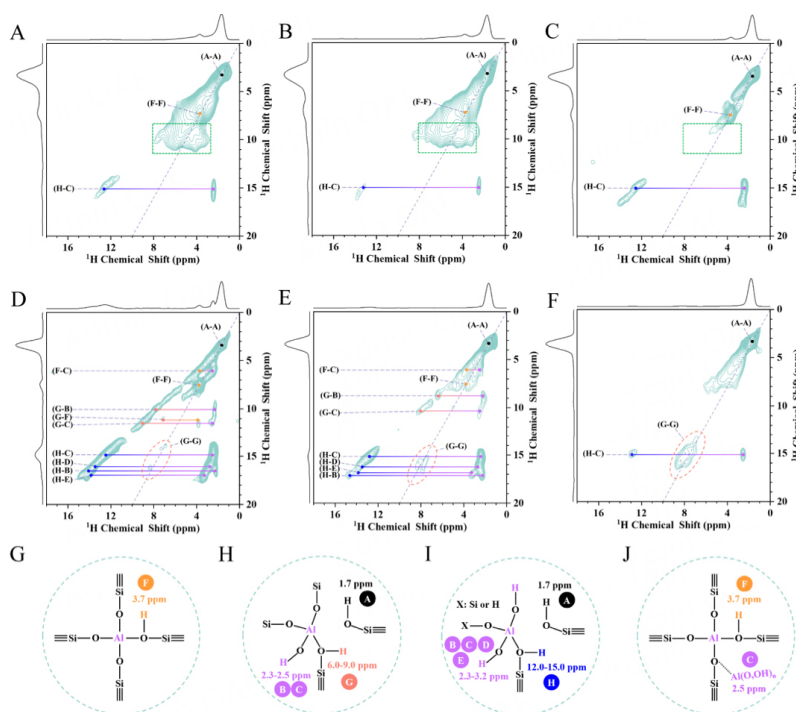
Figure 4. 2D ^{1}H-^{1}H DQ-SQ MAS NMR spectra of dehydrated HZSM-5 (A); HZSM-5-100-2 (B); HZSM-5-200-2 (C); HZSM-5-300-2 (D); HZSM-5-400-2 (E); HZSM-5-500-2 (F); (G-J) structure of proton signals with different ^{1}H chemical shifts where the letters from A to H corresponded to eight proton signals from the high filed to the low field, respectively.
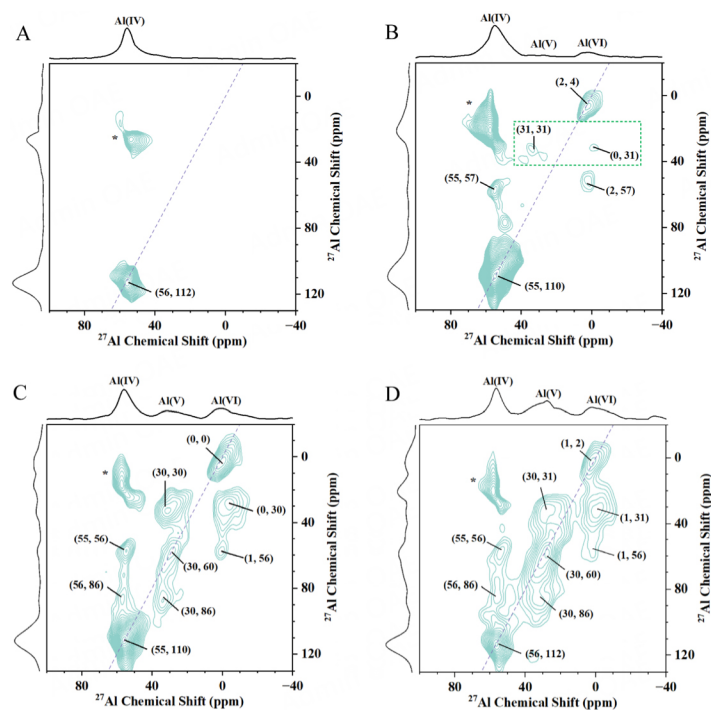

Figure 5. 2D ^{27}Al-^{27}Al DQ-SQ MAS NMR spectra of hydrated HZSM-5 (A); HZSM-5-300-24 (B); HZSM-5-400-2 (C) and HZSM-5-500-2 (D). All samples were fully hydrated.

that is inevitably generated during the calcination process for template removal. Compared to HZSM-5, after steaming at 100 °C and 200 °C, as shown in Figure 4B and C, no new autocorrelation and off-diagonal peak pair appear. Note that the green-doted region associated with the broad shoulder peak at 4.5-8 ppm disappears at 200 °C. This change may be the result of condensation of extensive hydrogen-bonded silanols, as corroborated by ^1H MAS NMR and FTIR [Figure 3A-C] above.

After steaming at 300 °C, the spectrum [Figure 4D] exhibits increased complexity. Apart from the four signals observed above, four new signals at approximately 2.3 ppm (B), 2.8 ppm (D), 3.2 ppm (E), and 6.0-9.0 ppm (G) are visible, which result in one weak autocorrelation peak and seven off-diagonal peak pairs being additionally observed. ^{27}Al MAS NMR spectra [Figure 1] have indicated that the framework Al-O bonds have been hydrolyzed to generate Al(IV)-2 species. Therefore, it is reasonably speculated that the four new signals (B, D, E, and G) are associated with Al(IV)-2 species. The off-diagonal peak pair (C-F) at (2.5, 6.2) and (3.7, 6.2) ppm can correspond to the correlation between Al-OH groups on Al(IV)-2 and unperturbed BAS. For broad signal at 6.0-9.0 ppm (G) adjacent to Al atoms in ^1H-^{27}Al S-RESPDOR [Figure 3D], this signal was detected in dehydrated HZSM-5 zeolites by ^1H-^{27}Al D-HMQC experiments and assigned to partially coordinated framework Al, Al(IV)-2[43]. An analogous broad signal appearing at 5.0-8.0 ppm in the ^1H MAS NMR spectrum of CHA-type zeolites is also observed by our group. This signal has been attributed to BAS perturbed by framework Al-OH[35]. In this work, the broad signal at 6.0-9.0 ppm (G) is assigned to the BAS on Al(IV)-2. Since the detailed structures of Al(IV)-2 are not single, it is reasonable to ascribe both broad signals at 6.0-9.0 ppm and 12.0-15.0 ppm to the BAS on Al(IV)-2. This can be supported by differences in spatial proximity to different protons in 2D ^1H-^1H DQ-SQ MAS NMR spectra [Figure 4D]. Considering that the BAS on Al(IV)-2 can be perturbed by framework Al-OH groups on Al(IV)-2 due to complex hydrogen bonding interactions, the broad signal at 6.0-9.0 ppm and 12.0-15.0 ppm may contain fewer and more Al-OH groups, respectively, as shown in Figure 4H and I. Correspondingly, the weak off-diagonal peak pair (F-G) at (3.7, 11.0) and (7.3, 11.0) ppm is attributed to the correlation between unperturbed BAS and hydrogen-bonded BAS of Al(IV)-2, which can be explained by partial hydrolysis of one of the two unperturbed BASs with spatial proximity. The new weak autocorrelation peak (G-G) at (7.0-8.0, 14.0-16.0) ppm corresponds to the spatial proximity of the Al(IV)-2, suggesting that small amounts of unperturbed BASs with spatial proximity are partially hydrolyzed simultaneously. Note that the broad signal at 6.0-9.0 ppm (G) is also proximate to the Al-OH groups at 2.3 ppm (B-G); therefore, it is speculated that the signal at 2.3 ppm (B) is also framework Al-OH groups in Al(IV)-2. Similarly, the four signals at 2.3 ppm (B), 2.5 ppm (C), 2.8 ppm (D), and 3.2 ppm (E) with spatial proximity to the broad signal at 12.0-15.0 ppm can also be attributed to framework Al-OH groups in Al(IV)-2. Importantly, unlike the signals at 2.3 ppm (B) and 2.5 ppm (C), the new Al-OH groups at 2.8 ppm (D) and 3.2 ppm (E) only have spatial proximity with the broad signal at 12.0-15.0 ppm (D-H and E-H), without another broad signal at 6.0-9.0 ppm (G), which also points more complex interactions between the signal at 12.0-15.0 ppm (H) and Al-OH groups. The diversity of Al-OH groups on Al(IV)-2 may be caused by the complex and variable chemical environment.

Moreover, the spectrum of HZSM-5-400-2 [Figure 4E] closely resembles that of HZSM-5-300-2 [Figure 4D]. Two subtle distinctions are noteworthy. Firstly, the off-diagonal peak pair (F-G) at (3.7, 11.0) and (7.3, 11.0) ppm disappears. Secondly, the autocorrelation peaks (F-F and G-G) at (3.7, 7.4) and (8.0, 16.0) ppm weaken and strengthen, respectively. These indicate that more Al(IV)-1 is partially hydrolyzed to form Al(IV)-2; that is, increasing the temperature can accelerate the irreversible hydrolysis process of framework Al-O bonds, aligning with the framework dealumination observed in ^{27}Al MAS NMR [Figure 1]. The initial Al(OH)$_3$·H$_2$O EFAL species, generated by removal of Al atoms from the framework, would evolve further by interacting with BAS within the zeolite channels[27,28]. As analyzed above, the

possibility that the signals at 2.3-3.2 ppm (B-E) come from EFAL species cannot be ignored, given the complexity of the structural and chemical environments of EFAL and Al(IV)-2 species, along with the limited resolution of ^{1}H NMR spectra. At 500 °C, many signals with spatial proximity vanish [Figure 4F], which is primarily because most of the Al(IV)-1 are completely hydrolyzed and eventually evolved into EFAL species with fewer hydroxyl groups through dehydration condensation. Obviously, during dealumination of HZSM-5 under steam conditions, the spatial proximities (or interactions) between various hydroxyl groups in structurally distinct Al species (Al(IV)-1, Al(IV)-2, and EFAL species) are exceptionally intricate.

Identification of spatial proximity of various aluminum species

To identify the spatial proximity (or interaction) among various aluminum species in both pristine and steamed HZSM-5 zeolites, a 2D ^{27}Al-^{27}Al DQ-SQ MAS NMR technique is applied, as shown in Figure 5. For untreated HZSM-5 zeolite [Figure 5A], only one autocorrelation peak at (56, 112) ppm is observable, indicating that the tetrahedrally coordinated framework Al species, Al(IV)-1, are in close proximity to each other, in accordance with the observation of autocorrelation peak of BASs in the 2D ^{1}H-^{1}H DQ-SQ MAS NMR spectrum [Figure 4A]. After steaming at 300 °C for 24 h, compared to Figure 5A, one additional autocorrelation peak and two off-diagonal peak pairs are clearly distinguished, as shown in Figure 5B. The emergence of autocorrelation at (2, 4) ppm indicates that six-coordinate EFAL species are in close proximity to each other. A cross-peak pair at (2, 57) and (55, 57) ppm is attributed to the correlation between six-coordinate EFAL species and Al(IV)-1, and another weaker cross-peak pair at (0, 31) and (31, 31) ppm corresponds to the correlation between six- and five-coordinate EFAL species. Yu *et al.* studied the dealumination mechanism of HY, HMOR, and HZSM-5 zeolites, combining ^{27}Al DQ MAS NMR and theoretical calculations, and proposed that it is a successive process[27,28]. To be specific, first, six-coordinate Al(OH)$_3$ EFAL species are generated from zeolite frameworks, and then five-coordinate Al(OH)$_2^+$ and four-coordinate AlOH^{2+} EFAL species are produced in sequence by eliminating one and two water molecules through interaction between Al(OH)$_3$ EFAL species and BAS. Strangely, no correlation between four- and five-coordinate Al species is observed in our work. These data suggest the six- and five-coordinate EFAL species are closer than the four- and five-coordinate EFAL species, which may be due to the evolution of the six-coordinate Al(OH)$_3$ EFAL species into the five-coordinate neutral AlO(OH) EFAL species in channels by removing one water molecule rather than the five-coordinate Al(OH)$_2^+$ EFAL species interacting with BAS, that is, the four-coordinate framework Al species. After steaming at 400 °C and 500 °C, the autocorrelations of the three kinds of Al species (four-coordinate framework Al, five- and six-coordinate EFAL) and the spatial proximity between any two of them are clearly observable in the spectra [Figure 5C and D], indicating that they are in close proximity to one another. This may contribute to the complex spatial proximity of various hydroxyl groups during dealumination.

Dynamic evolution path of HZSM-5 zeolite framework under steam treatment

Based on our experiment data, the dynamic evolution path of the HZSM-5 zeolite framework under mild and severe steam conditions is proposed, as illustrated in Scheme 1, mainly including framework dealumination [Path 1-5 in Scheme 1] and defect self-healing [Path 6-8 in Scheme 1]. Under mild steam conditions (T ≤ 200 °C), almost no dealumination occurs, but a large number of hydrogen-bonded silanols (silanol nests) inevitably generated during the synthesis and calcination process are condensed to form new framework Si-O-Si bonds [Path 6 in Scheme 1]. As the steam treatment gradually becomes more severe (T ≥ 300 °C), the framework Al-O bonds undergo irreversible hydrolysis with water molecules in the channels, resulting in the dynamic evolution of the framework tetrahedral Al atoms. Certainly, partially bonded framework (SiO)$_{4-n}$-Al(OH)$_n$ species, Al(IV)-2, generated through the partial hydrolysis of framework Al-O bonds is an important intermediate species in dealumination [Paths 1 and 2 in Scheme 1]. The newly generated bridge hydroxyl groups of Al(IV)-2 can be perturbed by the newly generated framework Al-OH
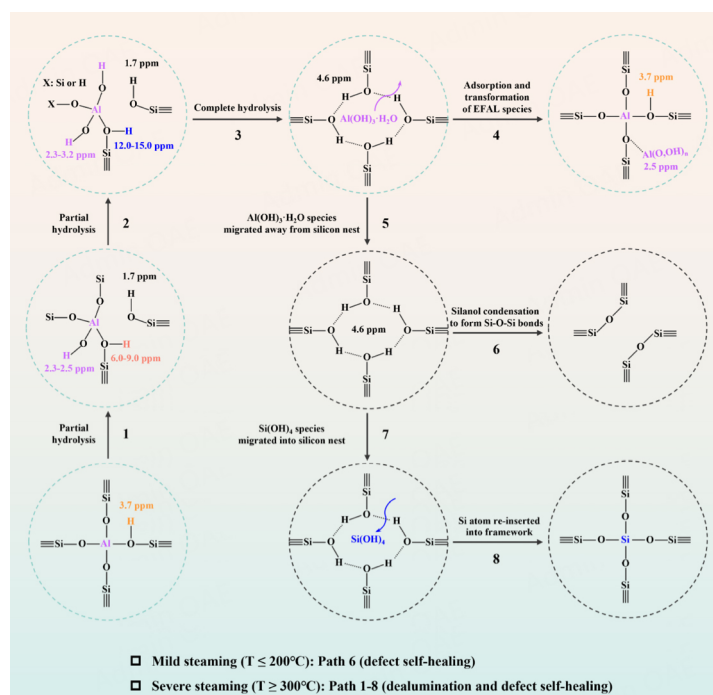
Scheme 1. Proposed dynamic evolution path of HZSM-5 zeolite frameworks under steam treatment.

groups due to hydrogen bonding interactions, which causes the ^{1}H chemical shifts to lower fields, appearing at 6.0-9.0 ppm and 12.0-15.0 ppm. When all four framework Al-O bonds bonded to one Al atom are completely hydrolyzed by four water molecules, the Al atom is completely removed from the framework, producing initial extra-framework $Al(OH)_3 \cdot H_2O$ species and silicon hydroxyl nests [Path 3 in scheme 1]. The $Al(OH)_3 \cdot H_2O$ species can subsequently migrate away from silicon nest [Path 5 in scheme 1] and transform into new EFAL species through hydroxyl condensation, such as $Al(OH)_2^+$, $Al(OH)^{2+}$, AlO^+, Al_2O_3, dimers, and trimers, which can be absorbed near the BAS by electrostatic interactions, stabilizing the framework but blocking the channel [Path 4 in Scheme 1]. In addition, the generated silanol nest will continue to evolve into new framework Si-O-Si bonds through condensation reactions of hydroxyl groups, including the direct condensation of adjacent Si-OH groups within silanol nests [Path 6 in Scheme 1] and the migration of $Si(OH)_4$ species produced by desilication to the silanol nest for reorganization [Paths 7 and 8 in Scheme 1]. Notably, during dealumination of HZSM-5 zeolite frameworks, these structurally distinct Al species coexist simultaneously, which complicates the spatial proximity of the different hydroxyl groups on them. Furthermore, the site specificity for steam-induced framework Al atoms removal in HZSM-5 zeolites has attracted much attention. Many studies have shown that Al atoms located at the intersections of straight and sinusoidal channels are more susceptible to dealumination, followed by sinusoidal channels, while Al atoms facing the straight channels are most stable[25,26,29,34].

CONCLUSIONS

In this study, the dynamic evolution of HZSM-5 (Si/Al = 36) zeolite frameworks and the spatial proximity of various hydroxyl groups and aluminum species under different steam conditions (ranging from 100 to 500 °C) are investigated qualitatively and quantitatively by carrying out XRD, SEM, FTIR, NH$_3$-TPD, N$_2$-physisorption in combination with 1D&2D ssNMR spectroscopy. As the steam temperature rises, the structure of HZSM-5 zeolite changes from orthorhombic to monoclinic symmetry, particularly at high temperatures. Under mild steam conditions (T ≤ 200 °C), although dealumination is nearly absent, the

silanol nests condense directly to create new framework Si-O-Si bonds. Conversely, under severe steam conditions (T ≥ 300 °C), the framework tetrahedral Al atoms can be completely removed from the framework, forming Al(IV)-2 and EFAL sequentially through partial and complete hydrolysis, which causes an increase in the framework Si/Al ratio and a decrease in crystallinity. Al(IV)-2 is recognized as a significant intermediate species for framework complete dealumination. The BAS of Al(IV)-2 can be perturbed by the framework Al-OH groups due to hydrogen bonding interactions, causing the ^{1}H chemical shifts to lower fields, appearing at 6.0-9.0 ppm and 12.0-15.0 ppm. The initial EFAL Al(OH)$_3$·H$_2$O species can be further transformed into new EFAL species, such as Al(OH)$_2^+$, AlO$^+$, AlO(OH), Al$_2$O$_3$, dimers, and trimers, through hydroxyl dehydration condensation, which can be absorbed on near the BAS by electrostatic interaction, stabilizing the framework but blocking the channels. Additionally, severe steam conditions may induce desilication, leading to the migration of Si(OH)$_4$ species to the silanol nest for reorganization. During dealumination, the spatial correlations (or interactions) of various hydroxyl groups on structurally distinct aluminum species [Al(IV)-1, Al(IV)-2, and EFAL] and aluminum species become extremely complex. Based on the above experimental results, the dynamic evolution path of HZSM-5 zeolite frameworks under mild and severe steam conditions is proposed, which contributes to a comprehensive understanding of host-guest interactions between zeolite frameworks and water molecules at the atomic scale.

DECLARATIONS

Authors' contributions
Designed the experiments, carried out characterization, analyzed data, interpreted results, drew the pictures, and wrote the manuscript: He LH
Synthesized samples: Li JJ, Li XJ
Conducted material characterization: Han SY, Fan D
Directed and supervised the project, analyzed data, and revised the manuscript: Xu ST
Analyzed data, contributed helpful discussions, and revised the manuscript: Wei YX
Provided administrative, technical, and material support: Liu ZM

Availability of data and materials
The data supporting this article have been included as part of the Supplementary Materials.

Conflicts of interest
All authors declared that there are no conflicts of interest.

Ethical approval and consent to participate
Not applicable.

Consent for publication

Not applicable.

Copyright

© The Author(s) 2024.

REFERENCES

1. Corma A. From microporous to mesoporous molecular sieve materials and their use in catalysis. *Chem Rev* 1997;97:2373-420. DOI
2. Davis ME. Ordered porous materials for emerging applications. *Nature* 2002;417:813-21. DOI
3. Dusselier M, Davis ME. Small-pore zeolites: synthesis and catalysis. *Chem Rev* 2018;118:5265-329. DOI
4. Chen LH, Sun MH, Wang Z, Yang W, Xie Z, Su BL. Hierarchically structured zeolites: from design to application. *Chem Rev* 2020;120:11194-294. DOI PubMed
5. Vogt ET, Weckhuysen BM. Fluid catalytic cracking: recent developments on the grand old lady of zeolite catalysis. *Chem Soc Rev* 2015;44:7342-70. DOI PubMed
6. Galadima A, Muraza O. Hydrocracking catalysts based on hierarchical zeolites: a recent progress. *J Ind Eng Chem* 2018;61:265-80. DOI
7. Tabak SA, Krambeck FJ, Garwood WE. Conversion of propylene and butylene over ZSM-5 catalyst. *AlChE J* 1986;32:1526-31. DOI
8. Ogunbadejo B, Aitani A, Čejka J, Kubů M, Al-Khattaf S. The effect of alkylation route on ethyltoluene production over different structural types of zeolites. *Chem Eng J* 2016;306:1071-80. DOI
9. Ono Y. Transformation of lower alkanes into aromatic hydrocarbons over ZSM-5 zeolites. *Catal Rev* 2006;34:179-226. DOI
10. Tian P, Wei Y, Ye M, Liu Z. Methanol to olefins (MTO): from fundamentals to commercialization. *ACS Catal* 2015;5:1922-38. DOI
11. Yang M, Fan D, Wei Y, Tian P, Liu Z. Recent progress in methanol-to-olefins (MTO) catalysts. *Adv Mater* 2019;31:e1902181. DOI PubMed
12. Liu Z, Huang J. Fundamentals of the catalytic conversion of methanol to hydrocarbons. *Chem Synth* 2022;2:21. DOI
13. Heard CJ, Grajciar L, Uhlik F, et al. Zeolite (In)stability under aqueous or steaming conditions. *Adv Mater* 2020;32:e2003264. DOI PubMed
14. Simancas R, Chokkalingam A, Elangovan SP, et al. Recent progress in the improvement of hydrothermal stability of zeolites. *Chem Sci* 2021;12:7677-95. DOI PubMed
15. Hu Z-P, Han J, Wei Y, Liu Z. Dynamic evolution of zeolite framework and metal-zeolite interface. *ACS Catal* 2022;12:5060-76. DOI
16. Resasco DE, Crossley SP, Wang B, White JL. Interaction of water with zeolites: a review. *Catal Rev* 2021;63:302-62. DOI
17. Stanciakova K, Weckhuysen BM. Water-active site interactions in zeolites and their relevance in catalysis. *Trends Chem* 2021;3:456-68. DOI
18. Smith L, Cheetham AK, Morris RE, et al. On the nature of water bound to a solid acid catalyst. *Science* 1996;271:799-802. DOI
19. Hunger B, Heuchel M, Matysik S, Beck K, Einicke WD. Adsorption of water on ZSM-5 zeolites. *Thermochim Acta* 1995;269-70:599-611. DOI
20. Randrianandraina J, Badawi M, Cardey B, et al. Adsorption of water in Na-LTA zeolites: an ab initio molecular dynamics investigation. *Phys Chem Chem Phys* 2021;23:19032-42. DOI PubMed
21. Heard CJ, Grajciar L, Rice CM, et al. Fast room temperature lability of aluminosilicate zeolites. *Nat Commun* 2019;10:4690. DOI
22. Pugh SM, Wright PA, Law DJ, Thompson N, Ashbrook SE. Facile, room-temperature (17)O enrichment of zeolite frameworks revealed by solid-state NMR spectroscopy. *J Am Chem Soc* 2020;142:900-06. DOI PubMed
23. Sun TT, Xu ST, Xiao D, et al. Water-induced structural dynamic process in molecular sieves under mild hydrothermal conditions: ship-in-a-bottle strategy for acidity identification and catalyst modification. *Angew Chem Int Ed* 2020;59:20672-81. DOI
24. Nielsen M, Brogaard RY, Falsig H, Beato P, Swang O, Svelle S. Kinetics of zeolite dealumination: insights from H-SSZ-13. *ACS Catal* 2015;5:7131-39. DOI
25. Silaghi MC, Chizallet C, Petracovschi E, Kerber T, Sauer J, Raybaud P. Regioselectivity of Al-O bond hydrolysis during zeolites dealumination unified by brønsted–evans–polanyi relationship. *ACS Catal* 2014;5:11-15. DOI
26. Silaghi M-C, Chizallet C, Sauer J, Raybaud P. Dealumination mechanisms of zeolites and extra-framework aluminum confinement. *J Catal* 2016;339:242-55. DOI
27. Yu Z, Zheng A, Wang Q, et al. Insights into the dealumination of zeolite HY revealed by sensitivity-enhanced 27Al DQ-MAS NMR spectroscopy at high field. *Angew Chem Int Ed* 2010;49:8657-61. DOI
28. Yu Z, Li S, Wang Q, et al. Brønsted/lewis acid synergy in H-ZSM-5 and H-MOR zeolites studied by 1H and 27Al DQ-MAS solid-state NMR spectroscopy. *J Phys Chem C* 2011;115:22320-27. DOI
29. Holzinger J, Beato P, Lundegaard LF, Skibsted J. Distribution of aluminum over the tetrahedral sites in ZSM-5 zeolites and their evolution after steam treatment. *J Phys Chem C* 2018;122:15595-613. DOI
30. Kalantzopoulos GN, Lundvall F, Thorshaug K, et al. Factors determining microporous material stability in water: the curious case of SAPO-37. *Chem Mater* 2020;32:1495-505. DOI
31. Zhang X, Cheng D, Chen F, Zhan X. Dealumination kinetics of composite ZSM-5/mordenite zeolite during steam treatment: an in-situ

DRIFTS study. *Chin J Chem Eng* 2018;26:545-50. DOI

32. Agostini G, Lamberti C, Palin L, et al. In situ XAS and XRPD parametric rietveld refinement to understand dealumination of Y zeolite catalyst. *J Am Chem Soc* 2010;132:667-78. DOI

33. Malola S, Svelle S, Bleken FL, Swang O. Detailed reaction paths for zeolite dealumination and desilication from density functional calculations. *Angew Chem Int Ed Engl* 2012;51:652-5. DOI PubMed

34. Stanciakova K, Ensing B, Göltl F, Bulo RE, Weckhuysen BM. Cooperative role of water molecules during the initial stage of water-induced zeolite dealumination. *ACS Catal* 2019;9:5119-35. DOI

35. Fan B, Zhu D, Wang L, Xu S, Wei Y, Liu Z. Dynamic evolution of Al species in the hydrothermal dealumination process of CHA zeolites. *Inorg Chem Front* 2022;9:3609-18. DOI

36. Bai X, Zhang J, Liu C, Xu S, Wei Y, Liu Z. Solid-state NMR study on dealumination mechanism of H-MOR zeolite by high-temperature hydrothermal treatment. *Micropor Mesopor Mat* 2023;354:112555. DOI

37. Ravi M, Sushkevich VL, van Bokhoven JA. Towards a better understanding of Lewis acidic aluminium in zeolites. *Nat Mater* 2020;19:1047-56. DOI PubMed

38. Wang Z, Wang L, Jiang Y, Hunger M, Huang J. Cooperativity of brønsted and lewis acid sites on zeolite for glycerol dehydration. *ACS Catal* 2014;4:1144-7. DOI

39. Zhao S, Yang W, Kim KD, et al. Synergy of extraframework Al^{3+} cations and brønsted acid sites on hierarchical ZSM-5 zeolites for butanol-to-olefin conversion. *J Phys Chem C* 2021;125:11665-76. DOI

40. Li S, Zheng A, Su Y, et al. Brønsted/lewis acid synergy in dealuminated HY zeolite: a combined solid-state NMR and theoretical calculation Study. *J Am Chem Soc* 2007;129:11161-71. DOI

41. Liu C, Li G, Hensen EJM, Pidko EA. Nature and catalytic role of extraframework aluminum in faujasite zeolite: a theoretical perspective. *ACS Catal* 2015;5:7024-33. DOI

42. Chen K, Horstmeier S, Nguyen VT, et al. Structure and catalytic characterization of a second framework Al(IV) site in zeolite catalysts revealed by NMR at 35.2 T. *J Am Chem Soc* 2020;142:7514-23. DOI PubMed

43. Chen K, Gan Z, Horstmeier S, White JL. Distribution of aluminum species in zeolite catalysts: (27)Al NMR of framework, partially-coordinated framework, and non-framework moieties. *J Am Chem Soc* 2021;143:6669-80. DOI PubMed

44. Chen K, Zornes A, Nguyen V, et al. (17)O labeling reveals paired active sites in zeolite catalysts. *J Am Chem Soc* 2022;144:16916-29. DOI PubMed

45. Yi X, Ko HH, Deng F, Liu SB, Zheng A. Solid-state (31)P NMR mapping of active centers and relevant spatial correlations in solid acid catalysts. *Nat Protoc* 2020;15:3527-55. DOI PubMed

46. Jaegers NR, Mueller KT, Wang Y, Hu JZ. Variable temperature and pressure operando MAS NMR for catalysis science and related materials. *Acc Chem Res* 2020;53:611-19. DOI PubMed

47. Wang W, Xu J, Deng F. Recent advances in solid-state NMR of zeolite catalysts. *Natl Sci Rev* 2022;9:nwac155. DOI PubMed

48. Hunger M. Multinuclear solid-state NMR studies of acidic and non-acidic hydroxyl protons in zeolites. *Solid State Nucl Magn Reson* 1996;6:1-29. DOI

49. Fyfe CA, Gobbi GC, Klinowski J, Thomas JM, Ramdas S. Resolving crystallographically distinct tetrahedral sites in silicalite and ZSM-5 by solid-state NMR. *Nature* 1982;296:530-33. DOI

50. Fyfe CA, Bretherton JL, Lam LY. Solid-State NMR detection, characterization, and quantification of the multiple aluminum environments in US-Y catalysts by 27Al MAS and MQMAS experiments at very high field. *J Am Chem Soc* 2001;123:5285-91. DOI

51. Zheng A, Liu SB, Deng F. Acidity characterization of heterogeneous catalysts by solid-state NMR spectroscopy using probe molecules. *Solid State Nucl Magn Reson* 2013;55-6:12-27. DOI PubMed

52. Li J, Liu M, Li S, Guo X, Song C. Influence of diffusion and acid properties on methane and propane selectivity in methanol-to-olefins reaction. *Ind Eng Chem Res* 2019;58:1896-905. DOI

53. Kabalan I, Michelin L, Rigolet S, et al. Influence of downsizing of zeolite crystals on the orthorhombic ↔ monoclinic phase transition in pure silica MFI-type. *Solid State Sci* 2016;58:111-14. DOI

54. van Koningsveld H. High-temperature (350 K) orthorhombic framework structure of zeolite H-ZSM-5. *Acta Cryst* 1990;46:731-35. DOI

55. van Koningsveld H, Jansen JC, van Bekkum H. The monoclinic framework structure of zeolite H-ZSM-5. Comparison with the orthorhombic framework of as-synthesized ZSM-5. *Zeolites* 1990;10:235-42. DOI

56. van Koningsveld H, Jansen JC, van Bekkum H. The orthorhombic/monoclinic transition in single crystals of zeolite ZSM-5. *Zeolites* 1987;7:564-68. DOI

57. Conner WC, Vincent R, Man P, Fraissard J. Flexibility in zeolites:29Si NMR studies of ZSM-5 frame transitions. *Catal Lett* 1990;4:75-83. DOI

58. Wu EL, Lawton SL, Olson DH, Rohrman AC, Kokotailo GT. ZSM-5-type materials. Factors affecting crystal symmetry. *J Phys Chem* 1979;83:2777-81. DOI

59. Geurts FMM, Kentgens APM, Veeman WS. 27Al nutation NMR of zeolites. *Chem Phys Lett* 1985;120:206-10. DOI

60. Hu JZ, Wan C, Vjunov A, et al. 27Al MAS NMR studies of HBEA zeolite at low to high magnetic fields. *J Phys Chem C* 2017;121:12849-54. DOI

61. van Bokhoven JA, Koningsberger DC, Kunkeler P, van Bekkum H, Kentgens APM. Stepwise dealumination of zeolite beta at specific T-sites observed with 27Al MAS and 27Al MQ MAS NMR. *J Am Chem Soc* 2000;122:12842-47. DOI

62. Frydman L, Harwood JS. Isotropic spectra of half-Integer quadrupolar spins from bidimensional magic-angle spinning NMR. *J Am Chem Soc* 1995;117:5367-68. DOI

63. Hu M, Wang C, Chu Y, et al. Unravelling the reactivity of framework lewis acid sites towards methanol activation on H-ZSM-5 zeolite with solid-state NMR spectroscopy. *Angew Chem Int Ed Engl* 2022;61:e202207400. DOI PubMed

64. Zeng S, Li J, Wang N, et al. Investigation of ethanol conversion on H-ZSM-5 zeolite by in situ solid-state NMR. *Energy Fuels* 2021;35:12319-28. DOI

65. Sivadinarayana C, Ganapathy S, Guisnet M, Choudhary VR. Resolution enhancement in the 29Si MASS NMR spectra of high silica ZSM-5. *J Catal* 1994;147:364-66. DOI

66. Hunger M, Ernst S, Steuernagel S, Weitkamp J. High-field 1H MAS NMR investigations of acidic and non-acidic hydroxyl groups in zeolites H-Beta, H-ZSM-5, H-ZSM-58 and H-MCM-22. *Microporous Mater* 1996;6:349-53. DOI

67. Chen K, Abdolrhamani M, Sheets E, Freeman J, Ward G, White JL. Direct detection of multiple acidic proton sites in zeolite HZSM-5. *J Am Chem Soc* 2017;139:18698-704. DOI PubMed

68. Treps L, Demaret C, Wisser D, et al. Spectroscopic expression of the external surface sites of H-ZSM-5. *J Phys Chem C* 2021;125:2163-81. DOI

69. Dib E, Costa IM, Vayssilov GN, Aleksandrov HA, Mintova S. Complex H-bonded silanol network in zeolites revealed by IR and NMR spectroscopy combined with DFT calculations. *J Mater Chem A* 2021;9:27347-52. DOI

70. Schroeder C, Siozios V, Hunger M, Hansen MR, Koller H. Disentangling brønsted acid sites and hydrogen-bonded silanol groups in high-silica zeolite H-ZSM-5. *J Phys Chem C* 2020;124:23380-6. DOI

71. Vayssilov GN, Aleksandrov HA, Dib E, Costa IM, Nesterenko N, Mintova S. Superacidity and spectral signatures of hydroxyl groups in zeolites. *Micropor Mesopor Mat* 2022;343:112144. DOI

72. Zhang WP, Ma D, Liu XC, Liu XM, Bao XH. Perfluorotributylamine as a probe molecule for distinguishing internal and external acidic sites in zeolites by high-resolution H-1 MAS NMR spectroscopy. *Chem Commun* 1999;12:1091-2. DOI

73. Schroeder C, Siozios V, Mück-Lichtenfeld C, Hunger M, Hansen MR, Koller H. Hydrogen bond formation of brønsted acid sites in zeolites. *Chem Mater* 2020;32:1564-74. DOI

74. Huo H, Peng L, Grey CP. Low Temperature 1H MAS NMR spectroscopy studies of proton motion in zeolite HZSM-5. *J Phys Chem C* 2009;113:8211-9. DOI

75. Ong LH, Dömök M, Olindo R, van Veen AC, Lercher JA. Dealumination of HZSM-5 via steam-treatment. *Micropor Mesopor Mat* 2012;164:9-20. DOI

76. Li J, Liu M, Guo X, et al. Influence of Al coordinates on hierarchical structure and T atoms redistribution during base leaching of ZSM-5. *Ind Eng Chem Res* 2018;57:15375-84. DOI

77. Jiao J, Altwasser S, Wang W, Weitkamp J, Hunger M. State of aluminum in dealuminated, nonhydrated zeolites Y investigated by multinuclear solid-state NMR spectroscopy. *J Phys Chem B* 2004;108:14305-10. DOI

78. Schallmoser S, Ikuno T, Wagenhofer MF, et al. Impact of the local environment of Brønsted acid sites in ZSM-5 on the catalytic activity in n-pentane cracking. *J Catal* 2014;316:93-102. DOI

79. Zecchina A, Bordiga S, Spoto G, et al. Low-temperature Fourier-transform infrared investigation of the interaction of CO with nanosized ZSM5 and silicalite. *J Chem Soc, Faraday Trans* 1992;88:2959-69. DOI

80. Omegna A, Vasic M, Anton van Bokhoven J, Pirngruber G, Prins R. Dealumination and realumination of microcrystalline zeolite beta: an XRD, FTIR and quantitative multinuclear (MQ) MAS NMR study. *Phys Chem Chem Phys* 2004;6:447-52. DOI